11-1-2023

Assessing the influence of glass properties on cabin solar heating and range of an electric vehicle using a comprehensive system model

A. K. Penning

Justin A. Weibel
jaweibel@purdue.edu

Penning, A. K. and Weibel, Justin A., "Assessing the influence of glass properties on cabin solar heating and range of an electric vehicle using a comprehensive system model" (2023). *CTRC Research Publications.* Paper 405.
http://dx.doi.org/https://doi.org/10.1016/j.apenergy.2023.120973

Assessing the influence of glass properties on cabin solar heating and range of an electric vehicle using a comprehensive system model[a]

Andrew K. Penning[1,2] and Justin A. Weibel[1,b]

[1]School of Mechanical Engineering
Purdue University
585 Purdue Mall, West Lafayette, IN 47907 USA

[2]3M – Transportation & Electronics Business Group Lab
3M Center
Maplewood, MN 55144 USA

Abstract

As consumer adoption and total energy consumption of electric vehicles continues to rapidly increase, it is important to develop comprehensive system modeling frameworks that consider the complex interactions of their mechanical, electrical, and thermal subsystems to guide component technology development. In this study, such a comprehensive system model of a generic long-range electric vehicle is developed and used specifically to assess the influence of cabin glass radiative properties on vehicle performance. The system model incorporates simplified models for all salient components in the electric traction drive, cabin HVAC, and battery subsystems, and uses a higher fidelity cabin thermal model that is able to capture the individual properties of the cabin glass used in the vehicle. The system performance is evaluated under a dynamic NEDC drive cycle which is repeated until battery depletion to determine a vehicle range. The system model is used to study five different glazing design cases, each corresponding to different transmission and reflection properties of the glass, by predicting their impact on the vehicle range. The cases span all theoretically possible glass properties while also enabling inspection of practical glass technologies that are available or under development to be adopted in modern electric vehicles. The influence of glass on vehicle range is then further compared at various locations across the United States to understand and illustrate the effects of ambient conditions and solar load. The system model predicts a vehicle range of 188.5 miles under a high solar loading scenario typical for Phoenix, AZ using traditional glass properties, which increases to a range of 221.6 miles using high-performance glass properties, representing a significant potential gain of 33.1 miles using technologies available on the market today. Under this same loading scenario, the glass properties at their extreme physical limits could theoretically affect the vehicle range by up to 92.5 miles. The influence of the glass properties is location-specific, and

[a] Submitted for possible publication in Applied Energy, 2022.
[b] Corresponding author, e-mail address: jaweibel@purdue.edu

the model predicts that using the same glass at different locations can affect the range of vehicle by up to 100.8 miles for traditional glass properties and 73.4 miles for high-performance glass properties.

Keywords

Electric vehicle; system modeling; glass properties; range prediction; HVAC; thermal management system.

Nomenclature

A_o	*Outer* Area [m^2]
A_i	*Inner* Area [m^2]
G	Solar irradiance [W/m^2]
m	Mass of vehicle [kg]
V	Volume of vehicle [m^3]
β	Glass solar property [-]
λ	Wavelength [nm]

Acronyms

AC	Air conditioning
ADS	Direct solar energy absorbed
CAGR	Compound annual growth rate
CFD	Computation fluid dynamics
COP	Coefficient of performance
EV	Electric vehicle
HX	Heat exchanger
HVAC	Heating, ventilation, and air conditioning
IR	Infrared
NEDC	New European drive cycle
NTU	Number thermal units
PID	Proportional integral derivative
PVB	Polyvinyl butyral
RDS	Direct solar energy reflected
SOC	State of charge
TDS	Direct solar energy transmitted
TXV	Thermostatic expansion valve

1 Introduction

Electric vehicle (EV) adoption has grown dramatically in recent years as the transportation industry is shifting from fossil-fuel-consuming internal combustion engines to electrified powertrains. *Research and Markets* predicts a Compound annual growth rate (CAGR) of 26.4% for electric vehicles by 2030 [1]. The COVID-19 pandemic has accelerated this transformation, as well as increasing the reliance on system models and component simulations to engineer new vehicles in a short time and to make informed techno-economic decisions at earlier design stages. In particular, the heating, ventilation, and air conditioning (HVAC) system efficiency has extremely important ramifications on performance, as the electrically powered vapor compression refrigeration subsystem consumes energy from the battery and thereby directly impacts the vehicle range. In many EVs, this thermal management system is relied upon to provide cooling for both the cabin as well as the battery pack, making the compressor draw the highest power compared to all other auxiliary components [2]. This compressor energy consumption can reduce driving range by 30% - 40% during a typical drive cycle [2]. There is significant current emphasis on reducing this energy consumption to increase vehicle range, either through efficiency improvements to the vapor compression system itself (e.g., waste heat recovery, compressor design, or advanced control strategies) or indirectly by developing technologies that will reduce the heating/cooling load (e.g., insulation materials, more efficient power conversion devices, or new battery technologies). Regardless of the approach, because the components in these electrical, mechanical, and thermal subsystems in the vehicle all interact to determine the total energy consumption, it is necessary to assess the potential performance benefit of any given technology using a comprehensive system model. The specific focus of the current work is on evaluating the effect of glass properties on cabin solar loading and thereby vehicle range using system model of a long-range electric vehicle.

In terms of understanding and representing the entire thermal management system, there are several foundational studies that have built generic EV modeling frameworks to probe various such research and development questions. Shelly et al. [3] recently developed a dynamic EV thermal management system simulation framework and showed that the range of a generic vehicle system can vary as much as 60 miles depending on ambient conditions. Shah et al. [4] also built a dynamic EV thermal management system model and specifically demonstrated that detailed component models could be included and co-simulated within the full thermal system framework. In regards to defining representative thermal management system architectures, Zhang et al. [2] has reviewed electric vehicle air conditioning (AC) system designs and described the challenges associated with mitigating their direct influence on vehicle range. Zhang et al. [5] also performed an experimental study on a particular system design with two evaporators in parallel flow paths, as it is becoming the most prevalent choice in EVs to provide cooling capacity for both the cabin and

the battery. The authors also identified how these evaporators interacted within such a parallel system, with their performance being interdependent on each other.

Additional separate research has been done to better understand cabin modeling strategies, and to assess the effect of cabin design parameters including glass properties. Warey et al. [6] used high-fidelity computation fluid dynamics (CFD) simulations to predict vehicle occupant thermal comfort. The high-fidelity model was then used to generate a training data set by varying glazing properties to build a machine learning surrogate model. This surrogate model developed was able to predict thermal comfort for any combination of boundary conditions and reduced the need to run the computationally expensive CFD simulations. Ruzic and Casnji [7] studied occupancy comfort in a tractor cabin and the thermal effects of glass glazing, concluding that the solar heat flux load is the largest energy source coming into the tractor cab. Soulios et al. [8] studied a parked car in a heating up scenario and showed how glass glazing can reduce the cabin air temperature by as much as 12.5°C using both experimental and numerical techniques. Combining research of the glass glazing properties with knowledge of the EV thermal system provides an interesting opportunity to design and optimize the properties of the glass glazing that is used in modern day vehicles.

When studying the effect of glass, the goal is rather obvious – to reflect as much solar energy as possible subject to any practical constraints and regulatory requirements. However, the challenge becomes quantifying the benefit of improved solar reflection, in particular a translation to the utmost performance metric of total vehicle range, to make informed techno-economic decisions during the design of a vehicle cabin. Many of the previous studies discussed above were focused on comprehensive modeling of the system architecture while assuming some properties for the glass; the other remaining studies focused on the glass and cabin design, but with a highly simplified representation of the EV thermal system. The current work bridges the gap between these past efforts by performing an extensive study spanning all theoretically possible glass properties and assessing their impact on vehicle range within a comprehensive modeling framework that represents all salient components in the EV thermal system. It is interesting to study the theoretical extremes of glass properties as well as properties that correspond with policy regulations and specific types of glass used in cars today. This approach bounds the effect of cabin glass on the EV thermal system in terms of vehicle range while also providing context for comparison between current technologies.

2 Modeling Approach

2.1 System architecture

The thermal management system for an electric vehicle comprises several complex fluid flow loop subsystems interfacing multiple electrical, mechanical, or thermal components; these flow loops interact with one another through various heat exchangers and control strategies. Aside from heat exchangers and valves, the primary components are the compressor in the refrigeration cycle that is used to cool the battery coolant and cabin air, a cabin air blow, and pumps that circulate coolant in two separate loops through the battery pack, electric motor, and additional supporting electronics. The cabin, with occupants that must kept in a state of thermal comfort, is also critical to the system performance and the focus of the work presented here. Each of these components and subsystems can and have been studied extensively using various experimental and simulation methods [3-5, 9-12]. The approach taken here, at the system level, includes thermal models representing each of the various components and their heat transfer interactions, but the level of complexity for each component is chosen as necessary to meet the goals of the study. In particular, to study the effect of glass properties, a higher fidelity cabin model is used that considers the detailed geometry and properties of the glass, while other components (such as the battery, electric motor, and electronics) are treated in a rather simple manner as heat sources according to their component efficiency and power demands of the drive cycle.

The thermal management system architecture in this modeling work was derived from inspecting various designs of long-range electric vehicles found in the A2mac1 resource [13]. Using these various designs as guidance, FIGURE 1 shows a system schematic used for this study that represents a generic norm of systems found in current EVs. This system comprises five separate fluid flow loops that exchange heat with one another. The flow path shown blue in FIGURE 1 is ambient air flow through the radiator, sometimes termed underhood air. This loop also includes the radiator fan and dissipates vehicle waste heat from both the electric motor cooling loop and the refrigerant vapor-compression loop to the ambient. An ethylene-glycol coolant loop (green) provides cooling for the electric motor and associated electronics components including the invertor, accessory power module, and charging module. Starting at the pump, coolant in this loop flows through the radiator which reduces the single-phase coolant temperature as heat is rejected to the ambient. Next in line, the coolant absorbs waste heat in a serial flow path through the invertor, which converts direct current to alternating current, the accessory power module, providing power to vehicle accessories, and the charge module. Because this loop has little coupled influence on the study of the glass, the heat generation from these components is simply modeled by specifying the temperature rise of the fluid based on the flow heat capacity rate. This simply equates to a heat generation of 180 Watts for each component. The last component in this flow path is the electric motor which propels the vehicle.

An electric motor efficiency model is used to determine the heat generation dependent on the speed and torque required of the drive cycle that is implemented into the model with a look-up map. The flow path shown red in FIGURE 1 is another ethylene-glycol coolant loop that addresses the battery pack thermal management. This loop includes an additional coolant pump and a plate heat exchanger connected to the vapor-compression refrigeration cycle. The waste heat from the battery pack is rejected first to the refrigerant and from there to the ambient underhood air. The cabin air loop (yellow) maintains thermal comfort within the EV cabin. This loop includes the HVAC blower, air side of the cabin evaporator, and the detailed cabin model itself. Lastly, the final flow path (purple) is the R134a refrigerant loop which includes the standard vapor compression cycle components: compressor, condenser, expansion valve, and in this case, two separate evaporators. Starting at the compressor exit, refrigerant flows through the condenser rejecting its heat and condensing from vapor to liquid. Next is a thermostatic expansion valve (TXV) which drops the pressure and temperature of the refrigerant before it flows through the two evaporators, one for the cabin air and the other for the battery coolant. Refrigerant flows in parallel through each evaporator at different flow rates and then recombines before it returns to the compressor as superheated vapor. These flow loops, components, heat exchangers together capture the overall energy balance of the thermal management system and is representative of architectures commonly seen in EVs today. It is important to note that this representation reduces the system to only those components necessary for operation in a cooling mode, so as to focus the scope of study on the effect the glass properties in a hot environment. Nevertheless, the authors acknowledge that operating in a heating mode is important to the overall operation of an electric vehicle; future work in this area could be extended to a system architecture that allows for study of glass properties in a heating mode scenario. Zhang et al. [2] and Shelly et al. [3] both describe system architecture variations when considering the heating mode of the EV in a cold ambient scenario, for which there is no single most representative architecture, but they do not study the influence of glass properties.

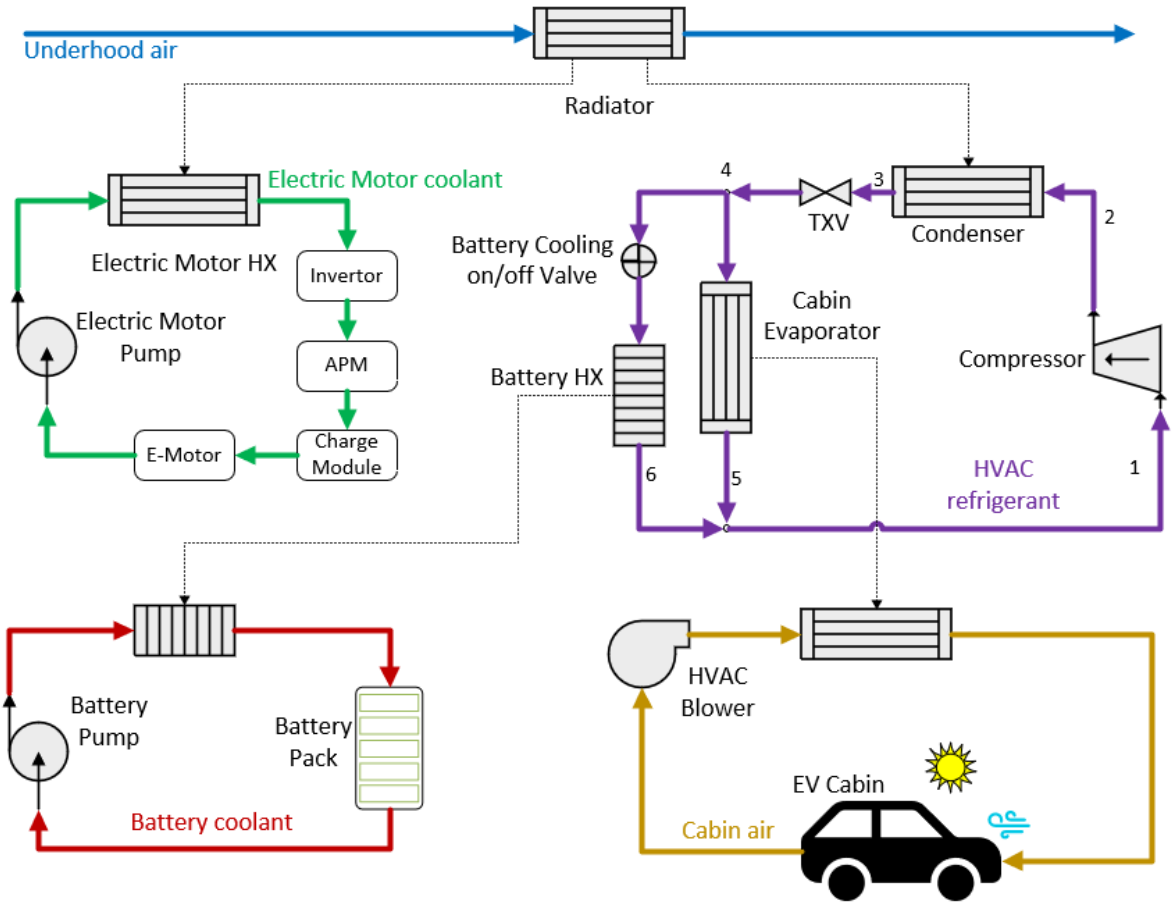

Figure 1: Schematic diagram of the thermal management system comprising multiple fluid flow loops and components in a manner representative of a common architecture in an electric vehicle. The loops are described in the text based on the fluid: underhood air (blue), electric motor coolant (green), battery coolant (red), cabin air (yellow), and HVAC refrigerant (purple).

The next Section 2.2 will describe the component models in more detail but briefly, within this system model, the various components are modeled as a collection of thermal masses and lumped fluid volumes. This common modeling assumption captures the energy balance and component interactions of the system with sufficient accuracy for system-level analysis, but the precise transient response and the internal temperature gradients are not captured. The exception is the cabin, which is modeled with enough resolution to account for effect of glass properties. The model is still based on a lumped thermal mass approach, but each wall within the cabin has its own thermal mass and external surface area. These thermal masses are thermally interconnected via radiation exchange and convection through the air volume of the cabin. The solar irradiance loading accounts for both transparent (glass) and opaque (roof/doors) walls with each part having its own absorptivity, transmissivity, and reflectivity value. Varying these properties for the glass while holding all other model parameters constant can isolate the influence of the glass properties on the thermal system and will be further discussed in Section 2.4. This cabin model was implemented into

the GT-Suite commercial software package using the Single Volume Cabin Model. Several components models such as thermal mass objects, heat exchanger objects, and flow volumes were utilized to build a custom model of the entire EV thermal system.

2.2 Component sizing and models

After determining the system architecture, each of the main components were sized appropriately to ensure sufficient cooling capacity for the vehicle. The vehicle would be typical of a long-range passenger SUV with a battery capacity of ~100 kWh. Table 1 summarizes the final dimensions of the heat exchangers used in the vapor compression cycle. The designs originated from components typically used in the automotive industry for the condenser, cabin evaporator, and battery heat exchanger (HX). The design parameters were then calibrated to ensure the system was not over or under sized for this specific system model. The heat exchanger modeling approach used within GT-Suite discretizes the heat exchanger into sections, using correlations to determine the rate of heat transfer within each section. This approach is computationally efficient while still capturing more resolution than a basic epsilon-NTU method. Comparing the final dimensions of these components to other sources in the literature [3], which were sized for a similar vehicle using a different software, confirms that the sizing for this current system is reasonable.

Table 1: Condenser, Cabin Evaporator, Battery HX Dimensions

	A_o	A_i	Length	Height	Depth
	mm^2	mm^2	mm	mm	mm
Condenser	3.140	0.868	480	370	12
Cabin Evaporator	2.646	0.608	160	275	44
Battery Evaporator	0.498	0.471	150	100	42

The R134a refrigerant loop was sized with a 115-cc variable speed compressor that can run from 0 to 4000 RPM, providing up to 5 kW of cooling capacity that is adequate for the battery and cabin across most cases. Throughout a drive cycle, the compressor can speed-up and slow-down depending on the cooling requirements of the cabin and battery. As the compressor size is kept constant in this analysis, there are some extreme ambient and setpoints at which the compressor is over or under-sized. While this introduces some bias into the results, we believe it is representative of a typical design decision wherein a single compressor is chosen for a particular vehicle model that must balance performance across these extreme scenarios. For example, designing a vehicle that will operate primarily in Phoenix, AZ would be different than a vehicle design for Washington State.

The cabin air volume and glass areas shown in Table 2 are input into the ‘Single Volume Cabin Model’ available within GT-Suite. This model is computationally efficient and can be solved actively

within the system framework, but still allows for capturing the effects of individual glass properties and surfaces. The air temperature is calculated as a single lumped volume and does not consider any temperature or velocity gradients in the cabin air volume. This single air volume is connected thermally, through convective heat transfer coefficient, to the walls within the cabin. This convective coefficient would be a function of the flow rate of air into the cabin; however, in this model it is simply assumed to be a constant value. The individual cabin walls are modeled as a single mass with 1D conduction effects included. These walls include all the various glass parts within the cabin, along with the roof, doors, and floor. Additionally, a cabin mass object is used to lump the seats, dash, and other interior components into a single part. This object has convective heat transfer to the cabin air through convective heat transfer and radiation to the other various cabin walls (which importantly captures secondary radiation effects). The solar irradiance calculations are included by manually calculating the orientation-dependent view factors and the optical properties of the transparent glass parts. The absorptivity of solar spectrum radiation (ADS) determines the amount of heat generation within an individual part while the solar transmissivity (TDS) determines how much energy is transmitted through the glass and to the cabin mass object. This cabin model is coupled to the system model through the cabin air loop.

Table 2: Cabin Dimensions

Parameter	Value	Unit
V_{air}	2492.5	L
$A_{windshield}$	1.0	m^2
$A_{sunroof}$	2.14	m^2
$A_{rear\ window}$	0.5	m^2
$A_{side\ windows}$	1.0	m^2

The battery details are outlined in Table 3. A Thevinin circuit is used to determine the heat generation within the battery pack. Because our study here is primarily interested in the heating load on the HVAC system, the model does not interrogate the detailed thermal dynamics of the battery pack, which is modeled as a single lumped mass. This masks all thermal gradient details that would be present in realistic battery pack of such a large mass; however, the battery model still captures temperature and state-of-charge (SOC) dependency of the heat generation and therefore required cooling capacity. The Thevinin circuit parameters used are from in Huria et al. [11] (see the section of the text titled *V. Modeling and Simulation*, *A. Look-up Tables* in this referred work). The study in [11] is for a high-power lithium battery chemistry and provides circuit parameters, voltage, resistance, and capacity, that are dependent on both battery temperature and SOC.

Table 3: Battery Pack Parameters

Parameter	Value	Unit
m	143	kg
Cell Capacity	31	Ah
N_{series}	105	–
$N_{parallel}$	8	–

All of these above-described component models coupled together through connections in the overall system model used for the analysis. This approach offers a high-level representation of capturing the many common features seen in modern electric vehicles. The system model was designed and implemented from scratch, with the response of each component and energy balance in each flow loop carefully inspected for correctness through various trial runs, as direct validation at the system-level is not possible for this fictitious generic vehicle. Even though direct validation to experimental data is not possible with this system model due to the lack of direct correspondence with a specific vehicle, the authors have cross-validated the dynamic system predictions with steady-state system analysis of the HVAC sub-system implemented in Engineering Equation Solver (EES) [13]. This was done by building a steady-state model of the HVAC sub-system and performing both thermodynamic analysis and component analysis. Thermodynamic analysis calculates the state points of the vapor-compression cycle and determines the heat rates from the specific enthalpy differences. The component analysis uses the epsilon-NTU method for the heat exchangers and determines specific enthalpy differences using energy balances. The models were cross-validated by ensuring all state points matched along with the heat and work rates for the condenser, evaporators, and compressor. This gave confidence that the model presented here is providing reasonable results.

2.3 Control scheme

With any thermal system of this complexity, a control scheme is necessary to control necessary interactions of the components to meet the various temperature set points throughout the system. A simple control scheme is taken here, relative to what would likely be found in a real vehicle, so as not to convolute interpretation of the system response to changes in glass. Specifically, the minimum necessary control intervention is included such that a reasonable battery temperature of 35 °C and a cabin air temperature of 20 °C are both maintained. Because maintaining cabin air temperature under various glass combination is the main goal of this work, system control tuning prioritized that the cabin air temperature be tightly maintained throughout the drive cycle

With this approach, the final control system includes four separate proportional–integral–derivative (PID) controllers and a single on-off valve. The first control point is the cabin air temperature to maintain thermal comfort, which is managed by the HVAC fan speed. The second control point is the cabin air inlet

temperature which is managed by the compressor speed. Thirdly, the compressor inlet superheat is maintained by controlling the TXV orifice size. Fourth, the battery temperature is maintained by the battery pump, meaning that the flow rate provided from the battery pump through the battery cold plate is controlled by the temperature of the battery. Lastly, an on-off valve is used to allow refrigerant flow through the battery evaporator whenever the battery pump is on. The other potentially controllable components, such as the electric motor pump and condenser fan are set to a constant value for flow rate or speed. All these controls together maintain thermal comfort in the cabin and the battery temperature. The PID tuning parameters used in the control scheme were found by adjusting the values until a constant cabin air temperature could be maintained by the system through the drive cycle. Because the battery on-off valve results in an abrupt change to the vapor-compression cycle, the PID control for the battery was designed to prevent rapid on-off switching of this valve. This allowed for more stable control of the vapor-compression loop at the sacrifice of over/under-shooting the battery pack temperature set point. Table 4 summarizes all the controlled components, the control point, and the set-point used for each control point.

Table 4: Control Scheme Details

Controlled Component	**Control Point**	**Set point**
HVAC blower	Cabin air temperature	20 °C
Compressor	Cabin air inlet temperature	5 °C
Thermal Expansion Valve (TXV)	Evaporator exit superheat	5 °C
Battery on/off valve	Battery pump speed	–
Battery pump	Battery temperature	35 °C

The thermal system is studied under a dynamic NEDC drive cycle scenario having the velocity trace shown FIGURE 2(a). Vehicle range is estimated by repeating the simulation of this drive cycle to deplete the battery from 0.95 state of charge (SOC) to 0.05 SOC and calculating how far the vehicle has traveled. FIGURE 2(b) shows a representative result for the SOC of the battery during a simulation. Using this repeating drive cycle, the vehicle drives for ~10 hours until the SOC is 0.05, and the distance traveled is noted as the predicted EV range. This method results in a time-periodic steady-state scenario to occur during which the complex dynamic behavior associated with the drive cycle is captured. Of the different methods to predict EV range, this method is simple and effective, at the expense of longer simulation time. It should be noted that the simulation runs at approximately twice real time, meaning for a ~10 hr range prediction, it takes ~5 hrs to solve.

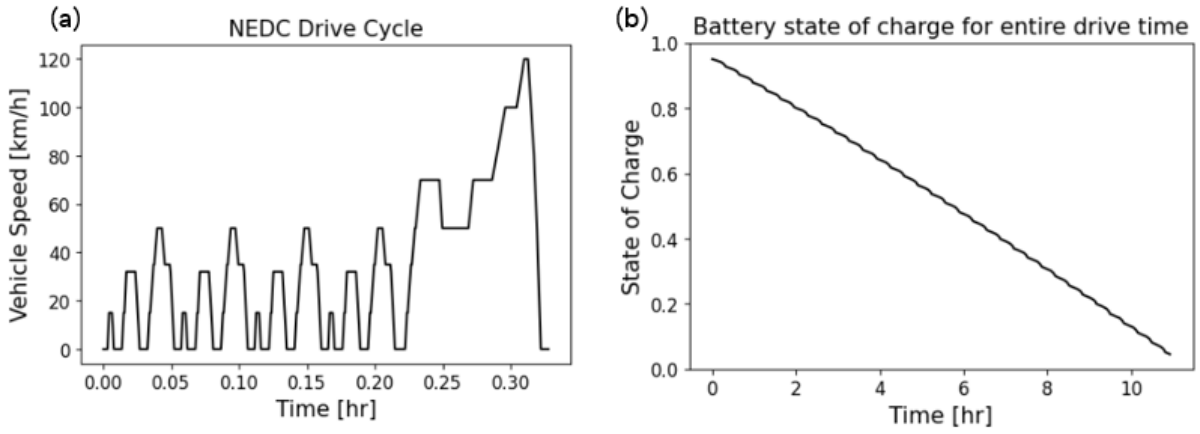

Figure 2: a) Vehicle speed versus time for the NEDC drive cycle. b) Battery state of charge (SOC) for a representative case of the full run time. Range prediction runs a repeating NEDC drive cycle and tracks the total distance traveled as the SOC depletes from 0.95 to 0.05.

2.4 Glass properties and test cases

In automotive glass that is used in vehicles today, there are typically 3-5 individual layers as shown FIGURE 3(a), two of which are the inner/out glass with some polyvinyl butyral (PVB) interlayer or other optical films in between. The type of glass along with the film properties can dramatically change the wavelength-dependent optical properties of the glass. Determining these composite glass properties can be done through optical modeling [15] or experimentally using a spectrophotometer. The objective of both methods is to provide the transmission and reflection properties as a function of wavelength, as shown for the example spectral transmission profile for a traditional glass glazing in FIGURE 3(b). These spectral radiation properties can then be converted to total properties (i.e., integrated over the spectrum) following the methods in ISO 13837 [16] or from Rubin et al. [17] and using the equation:

$$\beta_s = \frac{\int_0^\infty \beta_\lambda(\lambda) G_{s,\lambda}(\lambda) d\lambda}{\int_0^\infty G_{s,\lambda}(\lambda) d\lambda} \quad (1)$$

where, β_s is the laminate transmissivity or reflectivity, the subscript λ indicates whether it is a total value or a function of wavelength, and $G_{s,\lambda}$ is the solar irradiance as a function of wavelength as found in ISO 13987 [16]. This equation effectively provides a single glass transmissivity or reflectively as an average that is weighted by the solar spectrum. While such optical properties can be delineated by the individual glass layers, a common approach as taken here is to consider entire composite structure as a single layer with a single set of effective properties (transmissivity, reflectivity, and absorptivity). This sets a more useful

property target or reference for glass designers when they are exploring many different combinations of glass, PVB, and optical films.

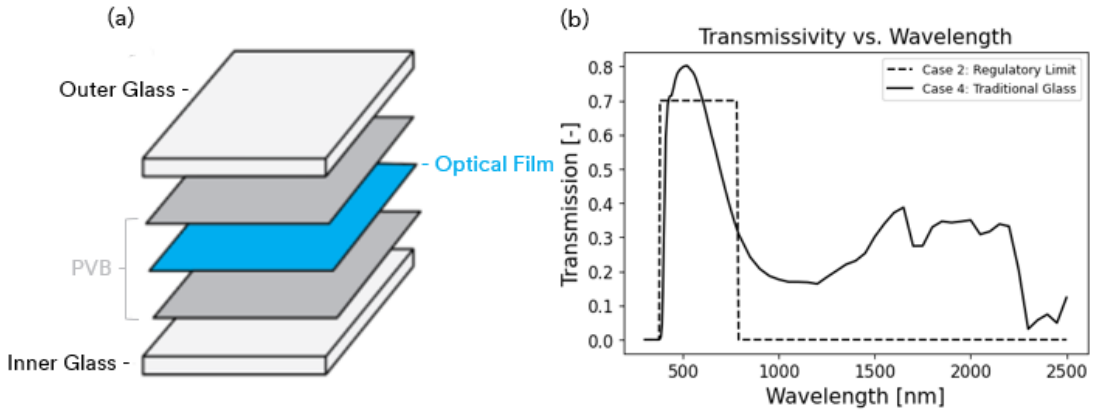

Figure 3: a) Schematic illustration of a typical automotive glass construction with two layers of glass on the outsides sandwiching two PVB layers and an internal IR-reflective film layer. b) Transmission spectrum for the traditional glass glazing and transmission spectrum that satisfies regulatory limit.

With this treatment, TDS refers to the amount of solar energy that is transmitted through the glass, RDS the solar energy reflected, and ADS the solar energy absorbed, which must sum to unity (TDS + RDS + ADS = 1).

To explore the influence of these glass properties on the thermal management system performance and vehicle range, six different test cases are established that have different combinations of optical properties that corresponds with practical scenarios of interest. The specific TDS, RDS, and ADS properties for each case are detailed in TABLE 4. To briefly summarize each: Case 1 represents a ‘physical limit’ at which all solar energy is reflected by all glass surfaces; Case 2 a ‘regulatory limit’ which ensures the required 70% visible light transmission through the windshield, side windows, and rear windshield (with the rest reflected), while the sunroof is entirely reflective; Case 3 represents a ‘high-performance glass’ which captures realistic properties for both the windshield and the roof glass having advanced IR rejection films; Case 4 represents the use of ‘traditional glass’ properties that would be typically found in vehicles today, having lesser reflection than the high-performance glass; case 5, where there is ‘no reflection (A)’ of the solar energy but 50% of the energy is absorbed and 50% is transmitted; and case 6: also with ‘no reflection (B)’, but all the solar energy is transmitted through the glass.

Case 1 is interesting because it provides a theoretical limit of the system that has no thermal loads associated with the glass performance. Case 2 is interesting because practically the driver needs to see out of the windshield and side windows in order to operate the vehicle. Additionally, it is interesting because it is a cabin design that would not have a sunroof incorporated. Cases 3 and 4 are interesting for practical reasons because they compare a high-performance glass representative of current state-of-the-art, to a

standard glass construction found in vehicles today. The high-performance glass (Case 3) has a five-layer glass construction (as was shown in FIGURE 3a) for both the sunroof and windshield; namely, the two pieces of glass on the outside sandwich an IR reflective layer between two PVB layers. In this case, the windshield and sunroof use different PVBs and IR reflective layers that optimize the properties for the intended application. For the Case 4: traditional glass (Case 4), the sunroof is a monolithic piece of glass while the windshield is a three-layer construction of a PVB layer sandwiched between glass on the outsides. Designers of EV cabins today have many choices in terms of glass layers; the range of different properties investigated across these cases can help inform how decisions regarding the construction of those layers will affect the thermal system response and vehicle range.

Table 4: Glass properties for each test case

		Sunroof			**Windshield**		
Case Name	**Case #**	**RDS**	**TDS**	**ADS**	**RDS**	**TDS**	**ADS**
Physical Limit	1	1.0	0.0	0.0	1.0	0.0	0.0
Regulatory Limit	2	1.0	0.0	0.0	0.617	0.383	0.0
High-performance	3	0.342	0.031	0.627	0.230	0.386	0.384
Traditional	4	0.044	0.164	0.792	0.054	0.435	0.511
No Reflection (A)	5	0.0	0.5	0.5	0.0	0.5	0.5
No Reflection (B)	6	0.0	1.0	0.0	0.0	1.0	0.0

3 Results and discussions

3.1 Range prediction method and baseline system response

The thermal system described above is studied under a baseline ambient condition defined as a hot ambient of 35 °C under direct overhead solar load of 1000 W/m^2, representative of conditions found in Phoenix, AZ. In a real scenario, the solar load and ambient temperature would fluctuate over time; however, they are assumed to be constant in this analysis. Initially, all components in the vehicle are at 20 °C, simulating a vehicle that is sitting in an air-conditioned garage. The vehicle is then immediately subjected to the hot environment and is required to maintain thermal comfort and battery cooling. Holding this baseline scenario fixed allows for a direct comparison between the glass designs.

The baseline results one glass design, the high-performance glass (Case 3), are shown to illustrate the thermal management system response. FIGURE 4 compiles the dynamic results of the model throughout the baseline scenario for Case 3, plotting the (a) battery pack temperature, (b) battery coolant flow rate, (c) cabin temperatures, and (d) refrigerant flow rates through the evaporators over the entire drive time of the vehicle. These results correspond to the battery SOC. Because the battery pack is initially below its set

point temperature of 35 °C, it takes a significant amount of time (several hours) to heat up the mass of the battery until the control system intervenes. Due to the lumped thermal mass representation of this battery pack, the heat-up time predicted is longer than would be expected compared to realistic conditions where thermal gradients are present. Nevertheless, at this point, at a time of 3 hrs into the repeating drive cycle, the system responds by opening the battery on-off value, allowing a non-zero refrigerant flow rate through the battery evaporator and turning on the battery pump to cool down the battery. On-off cycling of this battery evaporator valve maintains the battery to within 2.5 °C of the set point throughout the drive cycle. The time traces of the battery coolant flow rate highlights how the control scheme turns the battery pump on and off as needed to maintain this battery temperature. This in turn increases the cooling requirement and therefore increases the total refrigerant flow rate needed to both condition the battery and maintain thermal comfort in the cabin.

The cabin air temperature is maintained within less than 1 °C of the set point throughout the entire simulation time. The windshield and sunroof temperatures are notably higher and fluctuate with the vehicle speed as the convection on the outside of the vehicle changes. Overall, the simulation resulted in a predicted vehicle range of 221.6 miles for this case, which is reasonable for a long-range EV subject to this hot ambient condition under which there is a significant energy consumption due to battery and cabin conditioning.

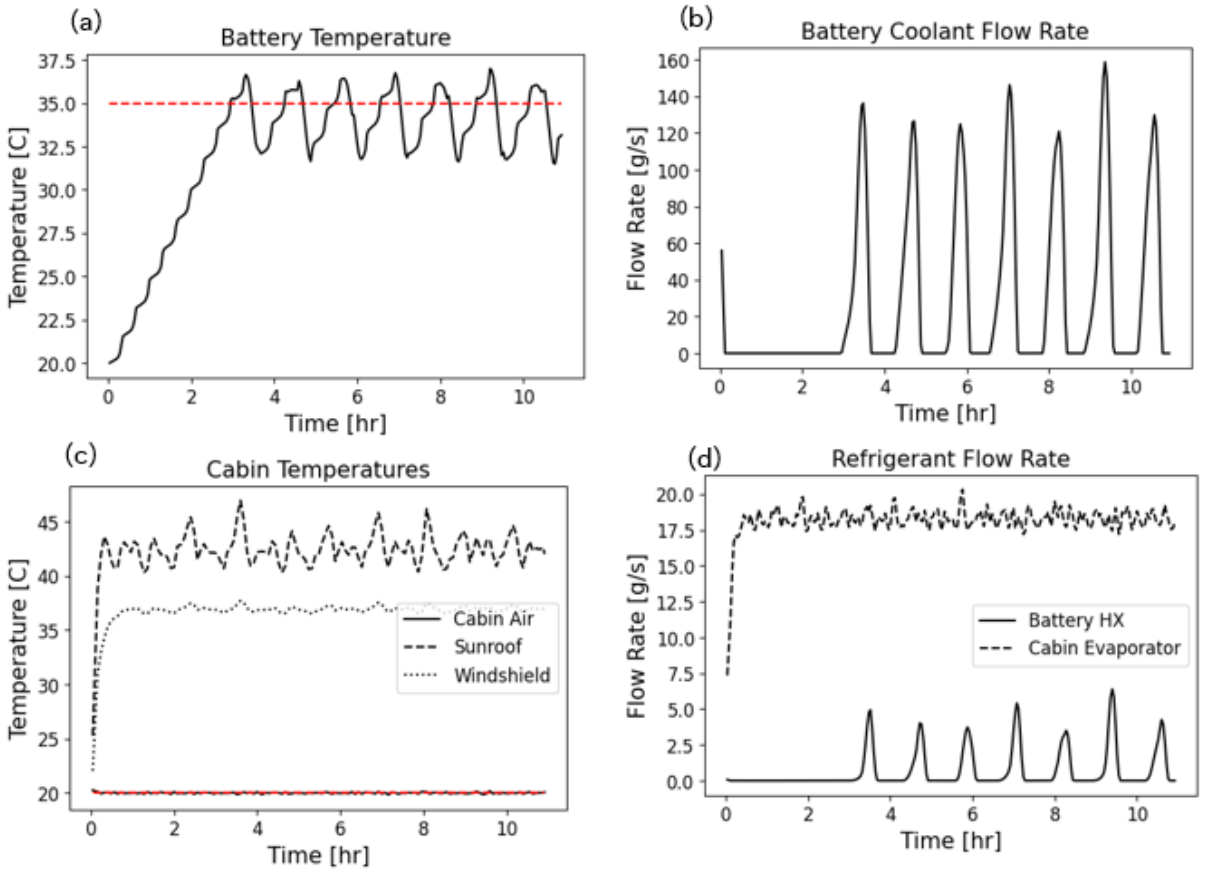

Figure 4: Dynamic system response throughout the drive cycle for the baseline ambient scenario under Case 3 (high-performance glass): a) average battery pack temperature; b) flow rate of coolant through the battery cold plate; c) cabin air, sunroof, and windshield temperatures; and d) refrigerant flow rate through the battery evaporator and the cabin evaporator.

Regarding the thermal management system energy consumption, inspecting the refrigerant flow rate in FIGURE 4(d) reveals that there is a significantly larger amount of flow directed toward the cabin evaporator, always at least 3 times more than the flow to the battery, and therefore much more of the compressor input power is needed for cabin versus battery conditioning. When the battery is heating up at the start of the system, no refrigerant flow is needed for the battery, and it all goes through the cabin evaporator. FIGURE 5 plots the compressor power draw and the battery and cabin cooling rates throughout the dynamic drive cycle. A large percentage of the cooling capacity is directed to the cabin, which remains relatively steady at ~2.5 kW, and only when battery cooling is needed does the battery HX have a relatively small spike in cooling rates up to ~0.5 kW. When this battery cooling need comes, the compressor responds by speeding up and providing additional cooling capacity. Integrating over the power usage data provides insight into the energy consumption for each of the various components. The percentage of energy used by each component is dependent on the glass design. For Case 3, high-performance glass properties result in

the electric motor and drive components using 70.5% of the total energy and 27.8% of the energy being consumed by the compressor. In comparison, Case 4 with traditional glass properties results in the electric drive system using 60% of the total energy and 37.8% of the energy is consumed by the compressor. The compressor is working harder when the glass is less effective at reducing the solar thermal load. Calculating a coefficient of performance (COP) as the total cooling rate divided by compressor power indicates a value of 1.3. While these results are for a specific Case 3 of high-performance glass properties, when studying different glass property cases in the later sections, the cabin evaporator cooling rates will change as the glass properties affect the cooling requirements of the HVAC system.

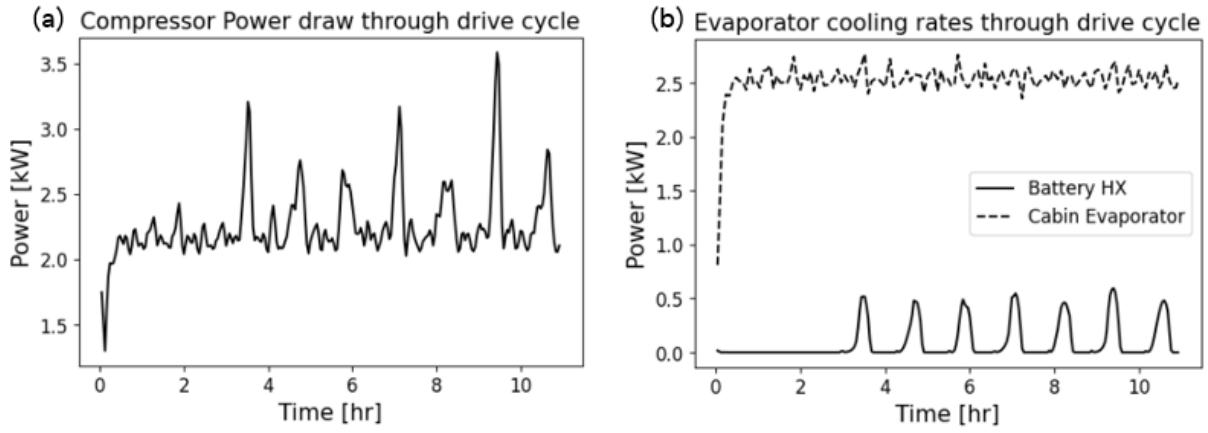

Figure 5: Dynamic system response throughout the drive cycle for the baseline ambient scenario under Case 3 (high-performance glass): a) compressor power usage; b) cooling rates for cabin evaporator and battery HX.

3.2 Influence of glass properties

For the given system design and all boundary conditions fixed at the baseline, the glass properties were swept over all theoretical combinations of transmission (TDS) and reflection (RDS) between 0 and 1 to explore the effect of cabin glass on the vehicle range. The absorption (ADS) can be inferred from the other properties; FIGURE 6(a) shows a contour plot of ADS for the complete range of TDS and RDS values explored for this virtual parameter sweep, the 4 different sets of glass in the cabin (namely, windshield, sunroof, side windows, and rear windshield) were all assigned the same properties.

FIGURE 6(b) shows contours of the predicted vehicle range. The most efficient, or maximum range, design is if all the incoming solar irradiance is reflected (RDS = 1). This effectively eliminates any cooling demands associated with solar loads being transmitted through or absorbed by the vehicle glass; the cabin cooling requirement is only due to heating by external convection with the ambient air. Under

these ideal conditions, the vehicle range was predicted to be 259.5 miles. Alternatively, the worst glass design is when all of the solar load is transmitted through the glass (TDS = 1.0) to the cabin interior; this results in a vehicle range of 167.0 miles. In the contour plot, there is a hashed region with TDS < 1.0 where the range is always at this minimum value; this is because, in this region, the HVAC system runs continuously at full capacity while still not being able to maintain the cabin set point temperature. This means that the system is undersized for these combinations of glass TDS and RDS properties. This exploration of the glass properties bounds their effect on this thermal system for the baseline hot ambient conditions, namely, a vehicle range difference of almost 100 miles. These results highlight an important point when considering design choices for an electric vehicle. While the physical goal is perhaps obvious, to reflect as much energy as possible, this comes with other practical and economic tradeoffs associated with improving the reflectivity of the glass. The results quantified in Figure 6(b), which shows how EV range varies with respect to reflectivity and transmissivity of the glass, can be used to assist in vehicle designers who are performing these techno-economic tradeoffs.

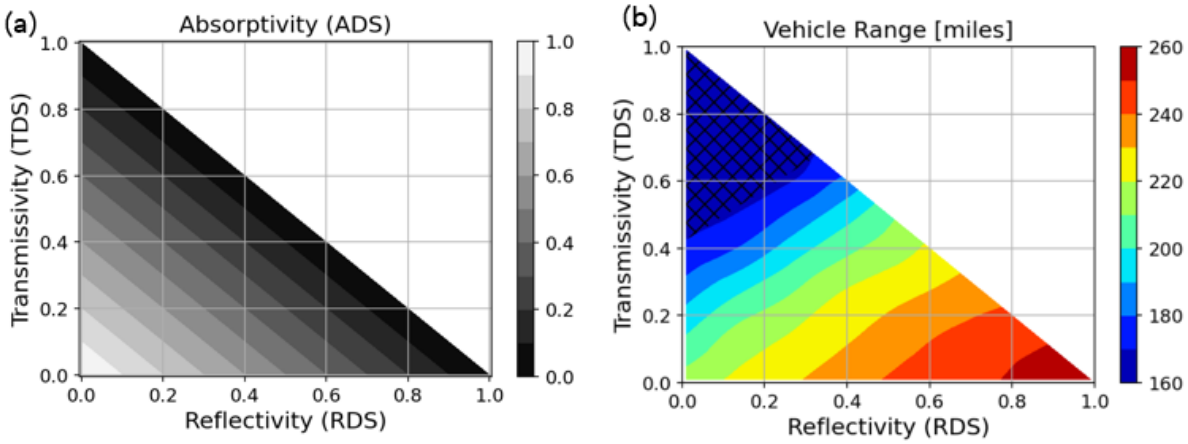

Figure 6: a) Relationship between the glass absorptivity (ADS), transmission (TDS), and reflection (RDS) over the range of all possible theoretical combinations. b) Predicted range of the vehicle as a function of these glass properties under the baseline ambient conditions of 35 °C and 1000 W/m^2.

With the range results predicted for all possible glass combinations, it is interesting to inspect the specific glass property combinations according to the cases introduced in TABLE 4 under the same hot ambient baseline conditions. FIGURE 7(a), overlays the properties of these cases as colored circular markers on top of the grayscale ADS contour plot showing the TDS and RDS design space; in cases where the sunroof has different properties from the rest of the glass, these properties are indicated by crosses. The predicted vehicle range for each case is plotted in the bar chart in FIGURE 7(b). The upper (Case 1: 259.5 miles) and lower (Cases 5&6: 167.0 miles) ranges correspond to the same extremes discussed in the previous paragraph. The next highest range of 247.4 miles correspond to the regulatory limit (Case 2)

because it allows for more energy to be transmitted through the windshield, side windows, and rear window based on visible light transmission regulation. This regulation effectively reduces range by 12.1 miles from the theoretical maximum. Considering more practical materials available today, the high-performance glass (Case 3) reduces the range by 37.9 miles compared to the theoretical maximum. A traditional glass (Case 4) reduces the range by 71.0 miles compared to the theoretical maximum, a penalty of 33.1 miles with respect to Case 3. This investigation shows that in theory there is up to a 100 mile range penalty when considering the glass properties. Additionally, the decisions that cabin and vehicle designers make in terms of choosing glass can result in a range difference of 33.1 miles under this hot ambient condition.

Considering these results, there is a direct relationship between glass reflectivity/transmissivity and EV range. This is because any solar energy not reflected is transmitted onto the internal cabin mass. The energy absorbed by this large mass is eventually transferred to the cabin air and therefore results in a corresponding increase in the cooling energy requirement based on the glass properties. Interestingly, this also implies that the absorptivity of the glass has a smaller influence. This may be expected because, although the surface of the glass is thermally connected to the cabin air, there is an alternative path to directly dissipate some portion of the heat absorbed by the glass to the surroundings, reducing the impact on the cabin load. This is demonstrated by looking at Figure 4(c); in this particular case, the glass temperature is indeed higher than the ambient resulting in a strong convective cooling of the glass to ambient.

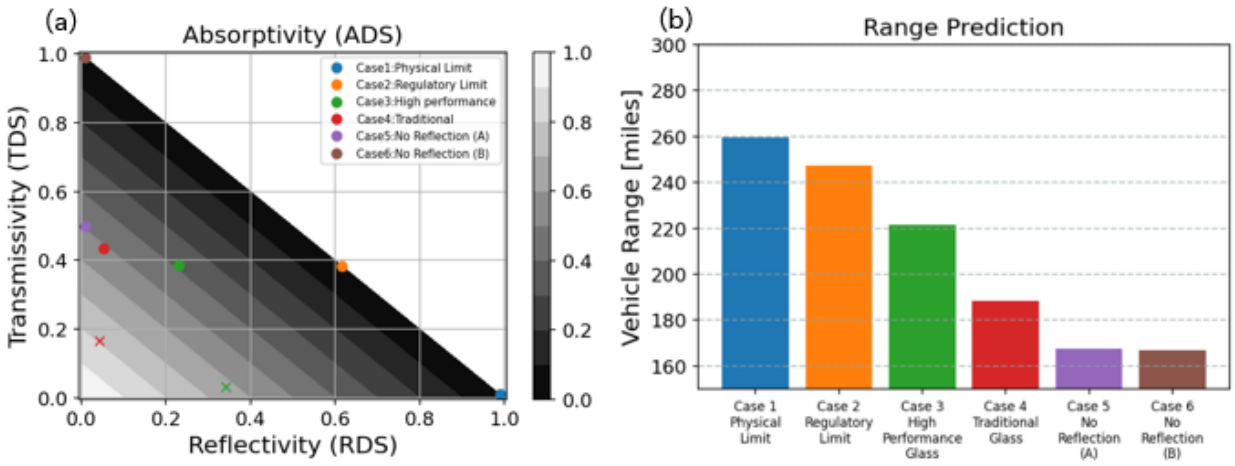

Figure 7: a) Individual glass properties (TDS, RDS, & ADS) for specific cases. b) Vehicle range prediction for individual cases under the baseline ambient conditions of 35 °C and 1000 W/m^2.

3.3 Influence of ambient solar flux and temperature

The results presented in Sections 3.1 and 3.2 have been under the rather extreme ambient loading scenario defined as the baseline, which will not be representative of the loading scenario for an electric

vehicle at all geographic locations. To study the performance of the system for different representative ambient conditions, solar irradiance and ambient temperature data are gathered from the National Solar Radiation Database (NSRBD) [17]. FIGURE 8(a) shows geographic contour map of the average solar flux over a year throughout the United States. This highlights how the solar loading requirements of the vehicle will change across the US. For this study of the current EV thermal management system, a summer condition is used at five selected locations. FIGURE 8(b) shows the ambient temperature and solar flux associated with each of these locations, which were chosen to capture a variety of conditions. The vehicle range was predicted at each of these cases for glass properties associated with the regulatory limits (Case 2) and traditional glass (Case 4). FIGURE 8(c) is a bar chart of the vehicle range predicted for both of these cases at each location.

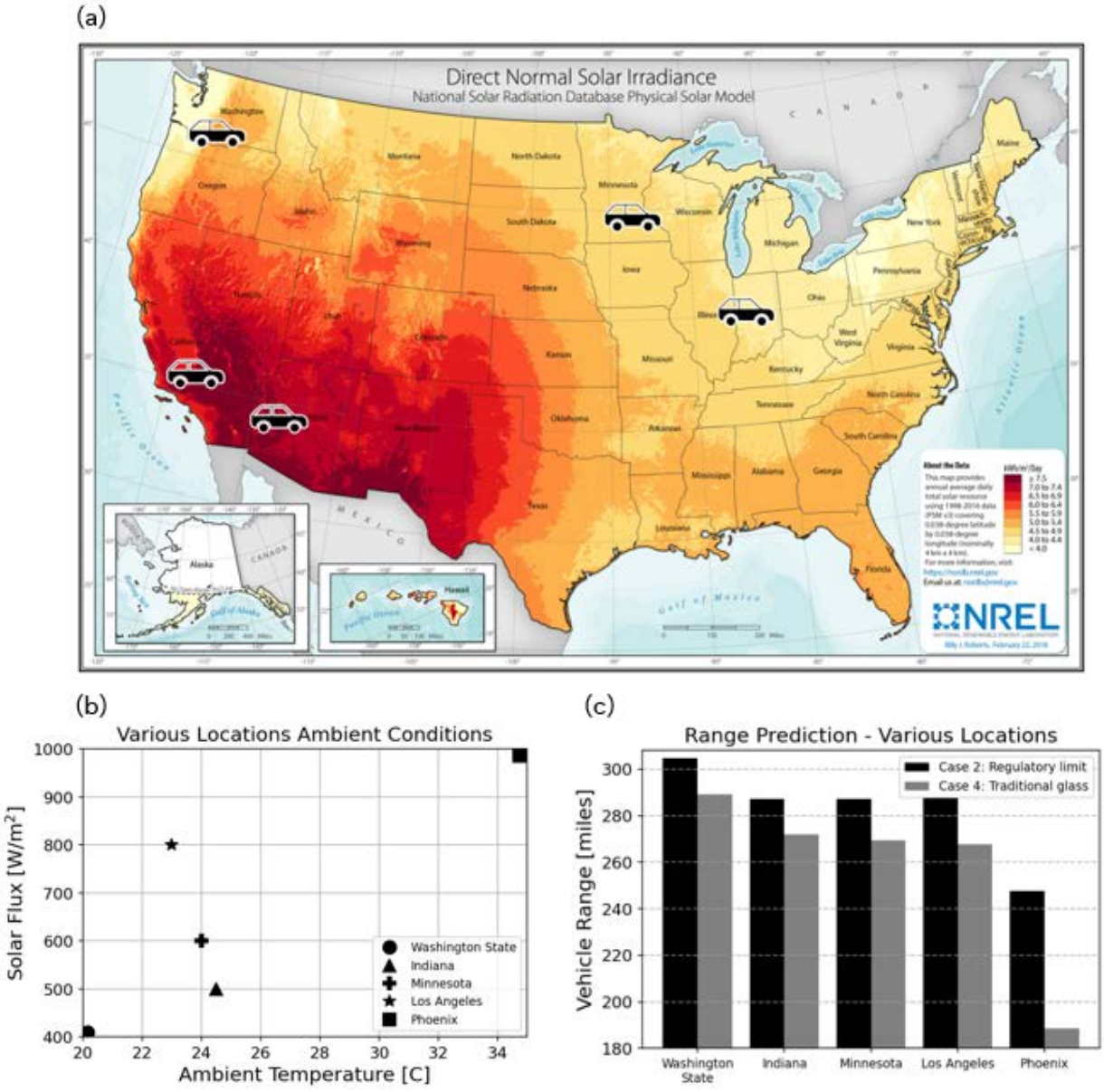

Figure 8: a) Direct normal irradiance across the US with locations studied (reproduced from [17]. b) Ambient conditions for the five locations studied. c) Range prediction for two glass cases based on the ambient conditions of the five locations.

The different ambient temperature and solar flux at each location results in different cooling requirements during the drive cycle. The extreme location, Phoenix, has a hot ambient of 35 °C and a large solar flux of 1000 W/m^2 (which corresponds to the 'baseline' above) while the gentle location, Washington State, has a low ambient temperature of 20 °C and a solar flux of 400 W/m^2. Inspecting the predicted ranges,

there is an almost 60 miles range difference between these extreme ambient locations when using the regulatory limit glass (from 304.7 miles in Washington State to 247.4 miles in Phoenix), and an even larger differences of 100 miles for the traditional glass case (from 289.2 to 188.5 miles). Interestingly, the other 3 locations of Indiana, Minnesota, and Los Angeles all result in similar range predictions despite their differences in solar flux and ambient temperature. This can be explained by the contour plots of predicted ranges shown in FIGURE 9, which sweep across all combinations of solar fluxes and ambient temperatures for the a) regulatory limit and b) traditional glass cases. The selected locations are indicated by black markers on top of the contours. The locations of Indiana, Minnesota, Los Angeles happen to lie on the same contour isolines of constant range for these specific glass properties due to the tradeoffs between solar flux and ambient temperature. These contours identify how the ambient temperature and the solar flux independently influence the performance of the HVAC system and affect vehicle range. Additionally, it can be inferred from the slope of the contour isolines that for increasingly reflective glass, the ambient temperature has a larger relative effect on the vehicle range because the solar loading is increasing negated by the glass. Conversely, as glass becomes less reflective, there is a greater dependency on the solar irradiance A broader takeaway is that the glass design decision is strongly influenced by the expected location of operation for the vehicle. The benefit of using a high-performance glass would be reduced, and possibly not worth the expected added vehicle cost, for operation in more moderate climates.

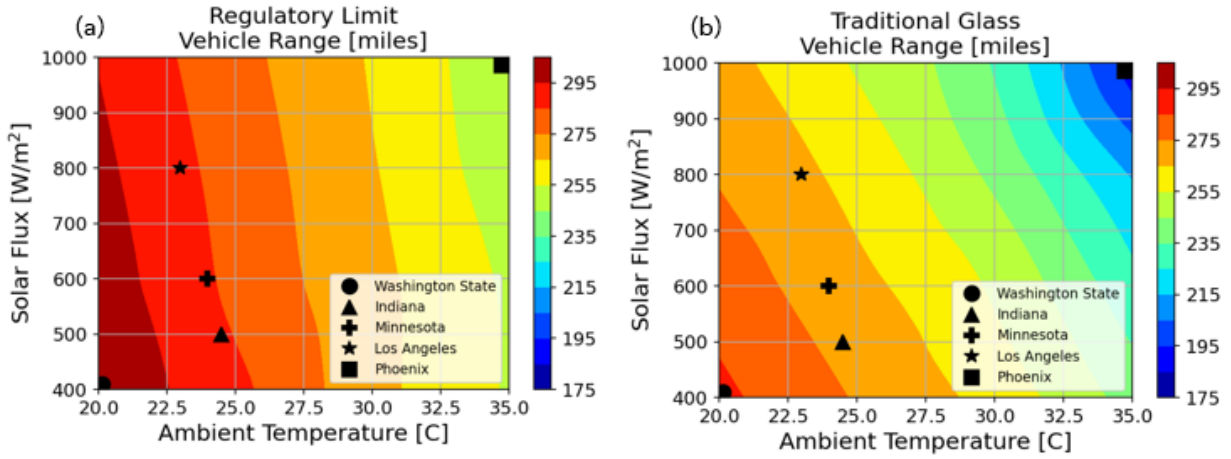

Figure 9: Vehicle range as function of ambient conditions with 5 locations marked. a) Range when using Case 2 (Regulatory Limit) glass properties. b) Range when using Case 4 (Traditional) glass properties.

4 Conclusions

In this paper, a thermal management system model was built to predict the driving range of a long-range electric vehicle. The system was designed generically to be representative of such vehicles found on the market today. With a focus on investigating the influence of glass properties on vehicle range, a modeling approach was taken that resolved the cabin in detail, while including simplified representations of the other components to capture the interactions and energy balance between all components in the full system. The baseline system response adequately controlled the cabin air temperature to a set-point of 20 °C and a battery temperature of 35 °C. Under a Phoenix, AZ loading condition of 1000 W/m^2 solar flux and 35 °C ambient temperature, the range prediction of the baseline system was 221.6 miles for high-performance glass and 188.5 miles for traditional glass. By varying the transmission and reflective properties of the cabin glass in all theoretical combinations, the model predicted that glass properties influence the vehicle range by 92.5 miles. Designing a cabin with the best glass properties given regulatory requirements, the vehicle range is reduced by 12.1 miles compared to the theoretical limit. Comparing high-performance glass to traditional glass results in 33.1 miles range variation. Lastly, the ambient conditions also influence the vehicle range prediction reducing this range variation from 33.1 miles for Phoenix, AZ to 5.8 miles for Washington State when changing from high-performance glass to traditional glass.

This work extensively studies the EV thermal system and cabin glass property considerations, but there are still many potential opportunities for future exploration. Such explorations could include system architecture changes, such as a detailed design and control scheme that would more closely resemble a specific vehicle on the road. The cabin model could be improved to capture velocity and temperature gradients that would be present in an EV cabin. Lastly, additional scenarios that include transient ambient conditions and angle-dependent optical properties could provide a very informative set of results for better understanding the influence of glass properties on the EV system.

The results in this study highlight the important of glass on the thermal management of the vehicle. It is critical to properly consider and represent the glass properties to ensure efficient system designs that have appropriated sized compressors, can maintain thermal comfort, and thereby maximum vehicle range. These large and complex systems have many component interactions, which requires a comprehensive model to predict the changes in performance and/or design requirements of the system in response to even minor property details. In the current study, it is shown that improvements to the radiative properties of glass have a potential for significant vehicle range increases within regulatory limits. The technoeconomic tradeoffs between these benefits to system performance and cost must also be thoroughly investigated.

Acknowledgements

The authors would like to thank 3M company for funding this work and providing the glass optical properties used in the study. Additionally, we acknowledge Gamma Technologies for providing software support for controls debugging and sizing considerations.

References

[1] R. and M. ltd, “Global electric vehicle market by component, vehicle (passenger cars, CV), propulsion (Bev, PHEV, FCEV), Vehicle Drive type (FWD, RWD, AWD), vehicle top speed (125 mph), charging point, vehicle class, V2G, and region - forecast 2030,” Research and Markets - Market Research Reports - Welcome. [Online]. Available: https://www.researchandmarkets.com/reports/5337979/global-electric-vehicle-market-by-component

[2] Z. Zhang, J. Wang, X. Feng, L. Chang, Y. Chen, and X. Wang, “The solutions to electric vehicle air conditioning systems: A review,” *Renewable and Sustainable Energy Reviews*, vol. 91, pp. 443–463, 2018

[3] T. J. Shelly, J. A. Weibel, D. Ziviani, and E. A. Groll, “A Dynamic Simulation Framework for the Analysis of Battery Electric Vehicle Thermal Management Systems,” in InterSociety Conference on Thermal and Thermomechanical Phenomena in Electronic Systems, ITHERM, 2020

[4] S. Shah, D. Vijay, and M. Lehocky, “Thermal management of electrified vehicle by means of system simulation,” *SAE Technical Papers*, 2020-28-0033, 2020

[5] G. Zhang, F. Qin, H. Zou, and C. Tian, “Experimental Study on a Dual- parallel-evaporator Heat Pump System for Thermal Management of Electric Vehicles,” in Energy Procedia, vol. 105, pp. 2390–2395, 2017

[6] A. Warey, S. Kaushik, B. Khalighi, M. Cruse, and G. Venkatesan, “Data-driven prediction of vehicle cabin thermal comfort: using machine learning and high-fidelity simulation results,” *International Journal of Heat and Mass Transfer*, vol. 148, 2020

[7] D. Ruzic and F. Casnji, “Thermal Interaction Between a Human Body and a Vehicle Cabin,” in *Heat Transfer Phenomena and Applications*, Chapter 11, M. S. N. Kazi, Ed. InTech, 2012

[8] V. Soulios, R. C. G. M. Loonen, V. Metavitsiadis, and J. L. M. Hensen, “Computational performance analysis of overheating mitigation measures in parked vehicles,” *Applied Energy*, vol. 231, pp. 635–644, 2018

[9] K. Olejniczak, T. Flint, D. Simco, S. Storkov, B. McGee, R. Shaw, B. Passmore, K. George, A. Curbow and T. McNutt, "A compact 110 kVA, 140°C ambient, 105°C liquid cooled, all-SiC inverter for electric vehicle traction drives," in IEEE Applied Power Electronics Conference and Exposition (APEC), Tampa, 2017

[10] S. M. N. Hasan, M. N. Anwar, M. Teimorzadeh, and D. P. Tasky, “Features and challenges for

Auxiliary Power Module (APM) design for hybrid/electric vehicle applications," in IEEE Vehicle Power and Propulsion Conference, VPPC, 2011

[11] T. Huria, M. Ceraolo, J. Gazzarri, and R. Jackey, "High fidelity electrical model with thermal dependence for characterization and simulation of high power lithium battery cells," in IEEE International Electric Vehicle Conference, IEVC, Greenville, 2012

[12] N. Doshi, D. Hanover, S. Hemmati, C. Morgan, and M. Shahbakhti, "Modeling of thermal dynamics of a connected hybrid electric vehicle for integrated hvac and powertrain optimal operation," in ASME Dynamic Systems and Control Conference, DSCC, 2019

[13] Klein, S.A. (2021) Engineering Equation Solver (EES) V11, F-Chart Software, Madison, USA. http://www.fchartsoftware.com

[14] A2MAC1. Automotive benchmarking platform, [Online]. Available: https://www.a2mac1.com/.

[15] Born, M.; Wolf, E., Principles of optics: electromagnetic theory of propagation, interference and diffraction of light. Oxford, Pergamon Press, 1964.

[16] International Organization for Standardization. *ISO 13837*. "Road vehicles – Safety glazing materials – Method for the determination of solar transmittance," 2008

[17] M. Rubin, K. von Rottkay, and R. Powles, "Window optics," *Solar Energy*, vol. 62, no. 3, pp. 149–161, 1998

[18] Sengupta, M., Y. Xie, A. Lopez, A. Habte, G. Maclaurin, and J. Shelby. 2018. "The National Solar Radiation Data Base (NSRDB)." Renewable and Sustainable Energy Reviews 89 (June): 51-60."

[19] S. Hemmati, N. Doshi, D. Hanover, C. Morgan, and M. Shahbakhti, "Integrated cabin heating and powertrain thermal energy management for a connected hybrid electric vehicle," *Applied Energy*, vol. 283, 2021

[20] A. Warey, S. Kaushik, and T. Han, "Physics-Guided Sparse Identification of Nonlinear Dynamics for Prediction of Vehicle Cabin Occupant Thermal Comfort," *SAE Technical Paper*, Vol. 1, 2022

[21] B. O. Varga, A. Sagoian, and F. Mariasiu, "Prediction of electric vehicle range: A comprehensive review of current issues and challenges," *Energies*, vol. 12, no. 5, pp. 946-965, 2019